J Digit Imaging (2015) 28:283–294
DOI 10.1007/s10278-014-9766-0

Staining Correction in Digital Pathology by Utilizing a Dye Amount Table

Pinky A. Bautista · Yukako Yagi

Published online: 6 January 2015

Abstract The stained colors of the tissue components are popularly used as features for image analysis. However, variations in the staining condition of the histology slides prompt variations to the color distribution of the stained tissue samples which could impact the accuracy of the analysis. In this paper, we present a method to correct the staining condition of a histology image. In the method, a look-up table (LUT) based on the dye amounts absorbed by the sample is built. The LUT can be built when either (i) the source and reference staining conditions are specified or (ii) when the user simply wants to recreate his/her preferred staining condition without specifying any reference slide. The effectiveness of the present method was evaluated in two aspects: (i) CIELAB color difference of nuclei, cytoplasm, and red blood cells, between the ten different slides of liver tissue, and (ii) classification of the different tissue components. Application of the present staining correction method reduced the color difference between the slides by an average factor of 9.8 and the classification performance of a linear discriminant classifier improved by 16.5 % on the average. Results of the paired *t* test statistical analysis further showed that the reduction in the CIELAB color difference between the slides and the improvement in the classifier's performance when staining correction was implemented is significant at $p<0.001$.

Keywords Staining correction · Color correction · Staining normalization · Digital pathology · Dye amount · Look-up table

P. A. Bautista (✉) · Y. Yagi
Department of Pathology, Massachusetts General Hospital (MGH), MGH PICT Center, 101 Merrimac, Suite 820, Boston, MA 02114, USA
e-mail: Bautista.Pinky@mgh.harvard.edu

Introduction

The burgeoning field of digital pathology has steered the development of automated image analysis systems as diagnostic accompaniment to pathologists [1–14]. Histopathology image analysis systems, when robustly designed, are attractive because they can provide diagnostic measurements which are reproducible. Object segmentation and classification processes are critical parts of an image analysis system as they handle the delineation of objects of interest from their background and the labeling of these objects to their appropriate classes. The performance of these processes are generally optimized using feature datasets collected from a set of training images identified beforehand.

Chemical staining impresses differing colors on tissue components having variations in their chemical makeup. In the implementation of a histopathology image analysis system, the colors of the stained tissue components are often considered as their segmentation or classification feature [4–13]. The issue in utilizing color for histopathology image analysis arises when the staining conditions of test and training images differ. Staining variations result to variations in the color distribution of the stained samples which could impact the accuracy of the analysis.

Integrating staining correction to the image analysis pipeline could improve its robustness from the staining variations in tissue slides. Methods to correct the staining condition of histological images have been presented in literatures [14–22]. Multispectral information was used by Abe et al. [15] to normalize the staining conditions of source images with respect to the staining condition of a reference slide. The reason behind using multispectral in the work of Abe et al. [15] was to obtain consistent results for digital staining where, in this process, similarly stained tissue structures have to be differentiated [14]. Without paying consideration to the differentiation of similarly stained tissue structures, the RGB colors of the

stained pixels were utilized instead by some groups. In the methods, pattern recognition algorithms were applied to derive an effective mapping of the stained RGB colors of the pixels in the source and reference slides [18–20]. The stain decomposition method proposed in [23] in conjunction with statistical pattern analysis has also been proposed [21, 22]. However, considering the image size of a high resolution whole slide image, the application of pattern classification procedures or the utilization multispectral information can be computationally expensive for the practical implementation of the staining normalization. Computationally expensive schemes could be made less expensive when hardware and software designs are optimized for the purpose. However, this could be counterbalanced by the increasing demand of users for higher image resolutions. Moreover, the present designs of whole slide image scanners are not configured for multispectral imaging applications. Also, there is no consensus yet to this date on the format for multispectral whole slide image.

The interplay between the amounts of dye absorbed by the tissue and its staining condition as demonstrated in [15] is suggestive of the notion that in drawing a framework for staining correction, it is more effective to utilize the amount of dye absorbed by the sample rather than its stained color. In this paper, we proposed a digital staining correction method by mapping the dye amounts absorbed by the source and reference tissue samples through a look-up table (LUT). Rather than utilizing multispectral information to determine the dye amounts in the stained pixels [15], the stain decomposition method presented in [23] is adopted to determine the dye amounts from the RGB color of the pixels. In the previous staining normalization approaches, the target staining condition is tied to the staining condition of the specified reference stained image and users do not have the option to recreate his/her preferred staining condition. On the contrary, in the present staining normalization approach, user will have the option to recreate his/her preferred staining condition by tweaking the entries of the dye amount LUT. Since there is a direct relation between the staining intensity of the tissue and the amount of dye it absorbed, i.e., the tissue expresses stronger staining intensity when it absorbs more dye, the user will find the proposed staining correction method more intuitive compared to previous methods which utilized the RGB colors of the image pixels. In this paper, we demonstrate how to estimate the dye amount LUT and how the user can modify such LUT to recreate his/her preferred staining condition. An advantage of the present approach, aside from featuring an option where user can actually recreate his/her preferred staining condition, is its more straightforward implementation and low computational complexity owing to the fact that it does not employ tissue classifications in the preliminary steps.

Method

Staining Correction Framework

Figure 1a illustrates the conceptual framework of our proposed staining correction method. It consists of three main parts: (i) conversion of the RGB color vector (R,G,B) to its dye amount vector (c_1,c_2,c_3); (ii) mapping of the pixels' dye amounts to their targets through the estimated LUTs; and (iii) visualization of the result in RGB color space. The LUT can be built from the dye amount tables derived from the specified source and reference slides, or from the dye amount table of the source slide alone. In the second case, the dye amount table for the reference staining condition corresponds to the dye amount table of the source slide which was adjusted so that the result recreates the staining condition preferred by the user.

Quantification of Dye Amount

According to Lambert-Beer law, the relation between light transmission and dye absorptions in stained samples can be expressed as follows [15]:

$$\mathbf{t} = exp(-\boldsymbol{\varepsilon}\mathbf{c}) \quad (1)$$

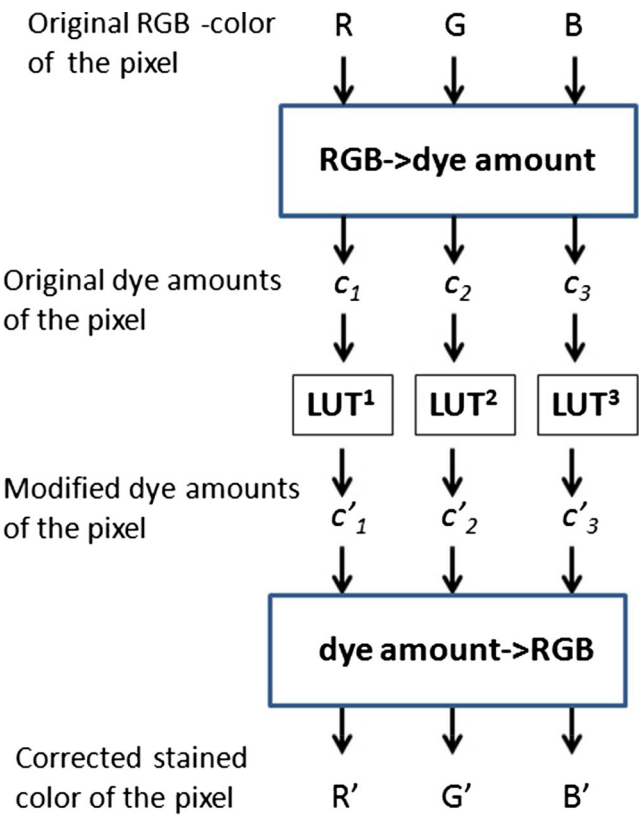

Fig. 1 Flow diagram of the staining correction using dye amount look-up table (LUT)

The variable **t** denotes the N-dimensional spectral transmittance vector of a pixel which is calculated as the ratio between the detected light I and the incident light I_o:

$$\mathbf{t} = \frac{\mathbf{I}}{\mathbf{I}_o} \tag{2}$$

Moreover, the notation $\boldsymbol{\varepsilon}$ in Eq. 1 is an $N \times P$-dimensional matrix containing the spectrum of the P dyes used to stain the sample, and **c** is a $P \times 1$ column vector whose elements are the concentrations of the P dyes in the sample. The optical density, A, of a material is equivalent to the logarithm of the light transmitted through it:

$$\mathbf{A} = -\log_{10}\left(\frac{\mathbf{I}}{\mathbf{I}_o}\right) \tag{3}$$

Let $\mathbf{I}=[I_R, I_G, I_B]^T$, $I_j \in \{0,255\}$, represents the RGB color channels gray-level intensities of a pixel. With the assumption that the gray-level intensities of the RGB color channels are linear to light transmission then the optical density of the pixel at the jth color channel, $j \in \{R,G,B\}$ can be computed as follows [21]:

$$A_j = -\log_{10}\left[\frac{Ij+1}{256}\right] \tag{4}$$

It can be easily established from the preceding equations that the optical densities of the pixels are linearly related to their stain concentrations and which can be compactly expressed in the following form:

$$\mathbf{A} = \mathbf{cM}, \tag{5}$$

The variables c and **A** are 3×1 vectors which, respectively, represent the stain concentration (or dye amounts) and the optical density of a color pixel, while the matrix M contains the normalized optical density (OD) matrix of the stain components. Let ε_{ij} denotes the absorption factor of the ith stain component in the jth color channel, the elements of matrix M are determined using Eq. 6 [23].

$$\widehat{\varepsilon}_{ij} = \frac{\varepsilon_{ij}}{\sqrt{\sum_{j=1}^{3} \varepsilon_{ij}^2}}, \quad i \in [\text{stain components}], j \in [\text{RGB color channels}] \tag{6}$$

The notation $\widehat{\varepsilon}_{ij}$ in the above expression represents the normalized absorption factor of the ith dye in the jth color channel. The pixel's dye amounts, c, can be determined by manipulating Eq. 5 yielding:

$$\mathbf{c} = \mathbf{AD} \tag{7}$$

where $\mathbf{D}=\mathbf{M}^{-1}$ and which we referred to as the deconvolution matrix.

Estimation of the Dye Amount LUT

The transformation of the pixel's original dye amounts **c** to its target dye amounts **c′** can be described by the function Φ:

$$\mathbf{c} = \Phi\left[\mathbf{c}'\right] \tag{8}$$

The idea of a LUT is to implement the transformation in Eq. 8 by mapping the input $\mathbf{c} \in \mathbf{Q}$ to its output $\mathbf{c}' \in \mathbf{S}$ using discrete sample data points in **Q** and **S** [24]. An overview on the derivation of the dye amount LUT when the target staining condition is represented by a reference slide is described as follows:

1. Specify the source and reference slides. Herein, the staining condition of the source slide will be corrected toward the staining condition of the reference slide.
2. Manually select areas from the whole slide images of the source and reference slides.
3. Calculate the image pixels' dye amounts using Eq. 7.
4. Determine the maximum, c_{max}, and the minimum dye amount, c_{min}, values for each of the stain component, c.
5. Determine the elements of the dye amount table by dividing the dye amount range of each stain component by n: $\frac{(c_{max}-c_{min})}{n}$, where n is the desired length of the table.
6. The dye amount LUT for the cth stain component is defined by the pair $[X^c, Y^c]$ where X^c and Y^c are the respective dye amount tables for the source and reference slides. They consist of n elements of equally spaced amount values ranging from c_{min} to c_{max}.

RGB Color Reconstruction

The RGB color composite of the corrected hematoxylin and eosin (H&E)-stained image can be determined by combining Eqs. 4 and 5:

$$\widehat{\mathbf{I}}_{RGB} = 255 * \left[10^{-\widehat{\mathbf{cM}}}\right] \tag{9}$$

The notation $\hat{\mathbf{I}}_{\mathrm{RGB}}$ and $\hat{\mathbf{c}}$ correspond, respectively, to the estimate of the pixel's target RGB color, $\hat{\mathbf{I}}_{\mathrm{RGB}} = \left(\hat{\mathrm{R}}, \hat{\mathrm{G}}, \hat{\mathrm{B}}\right)$, and their target dye amounts. Furthermore, the matrix M contains the dye absorption coefficients of the stain components.

Experiments and Results

Absorption Factors of the Stain Components

In this work, the RGB color of an H&E-stained pixel was decomposed into three stain components, namely, hematoxylin (H), eosin (E), and the unstained red blood cell (R) which was mainly considered due to the presence of hemoglobin color pigments in unstained tissue samples [15]. We utilized the spectral absorptions of the H-only stained nuclei, E-only stained cytoplasm, and unstained red blood cell (R) which we collected from the 63-band multispectral images of the H-only, E-only, and unstained tissue samples to determine the absorbance factors of these stain components. To acquire the multispectral images of these samples, we used the Olympus microscopic multispectral imaging system (Olympus, Japan) which is equipped with tunable filters which have spectral sensitivities within the visible spectrum. The imaging system also comes with viewer software that enables the user to select sample points from the captured 1434×1050 multispectral images [25]. Each stain component was represented with the average spectrum of the five spectral samples which we extracted from its corresponding multispectral image. We then determined the RGB color channel absorbance factor, ε_{ij}, of a stain component from the linear RGB color equivalent of its representative spectrum [15].

Image Sets

We retrieved ten whole slide images of H&E-stained liver tissue slides, which were scanned at a pixel resolution of 0.46 mM/pixel and at 80 % compression ratio using the Nanozoomer whole slide scanner, from the archive of the Massachusetts General Hospital (MGH) Pathology Imaging and Communication Technology (PICT) center. These slides were stained at different times and in different batches by different person. The viewer software of the whole slide scanner allows the user to annotate areas of interest as well as export the corresponding images of these areas in JPEG format. The software does not implement color correction to the scanned images. It does provide, however, the option to manually adjust the color channel intensities of the image pixels which we did not utilize in our experiments. We used the scanner viewer to randomly sample 20 areas from the whole slide images and then exported the 1280×960-pixel images of the areas in JPEG format.

Staining Variations in Tissue Images

The images in Fig. 2 demonstrate the existence of staining variations in different batches of histology slides. The images at the first row, Fig. 2a–c, are the low-resolution (thumbnail) versions of the high-resolution H&E digital slides. The images at the second row, Fig. 2d–f, are the high-resolution images (20×) of an area sampled from the digital slides of the H&E-stained sections in Fig. 2a–c. Moreover, the images at the third and fourth rows, Fig. 2g–i and Fig. 2j–l, are the RGB color representations of the H and E stain components of the RGB color images presented at the second row. H&E staining impresses pinkish to reddish color to tissue components which react mainly to E dye and purplish to bluish color to tissue components which react mainly to H dye. We can observe that the stained RGB colors of the samples are directly affected by their dye absorption characteristics. For instance, consider the image from slide #5. Its H image appears to have stronger color intensity than its E image implying that the sample absorbs more amount of H dye than E dye. We can see that the stained RGB color of slide #5 image, Fig. 2b, shows dominance to purplish hue which is the inherent staining color of H dye. On the contrary, the H&E-stained image of slide #1 shows dominance of pinkish hue associated to the staining color of E dye.

Estimation of the Dye Amount 1-D LUT

The crucial part in estimating the dye amount LUT for a given batch of slides is the determination of the appropriate values for the maximum and minimum dye amounts, $c_{\max}$ and $c_{\min}$. Noting that areas in the slide which do not contain any tissue structures are not stained, it was seen fitting to set $c_{\min}=0$. On the other hand, to avoid assigning $c_{\max}$ to spurious pixels which have abnormally higher dye amount content compared to the majority of the image pixels, $c_{\max}$ was determined by taking into consideration the statistical mean and standard deviation of the stained pixels' dye amount distribution. Specifically, we determined $c_{\max}$ by the following:

$$c_{\max} = \mu_c + k_c \sigma_c \tag{10}$$

where μ_c and σ_c, respectively, refer to the statistical mean and standard deviation of the stained pixels' dye amounts for the cth stain component. The variable k_c, is a real number, $k_c \in \Re^+$, and $k_c \geq 0$, which we set to a default value of 2. We noted that for some slides, the maximum dye amount is around 2, and so, we specified the length of the dye amount table to be $n=21$ such that dye amount entries in the table are incremented by around 0.10 or less. That is, we designed the LUT to consist of $n=21$ elements spaced at equal intervals from $c_{\min}$ to $c_{\max}$. The accuracy of the dye amount estimation can be affected by the length of the LUT; however, we found that

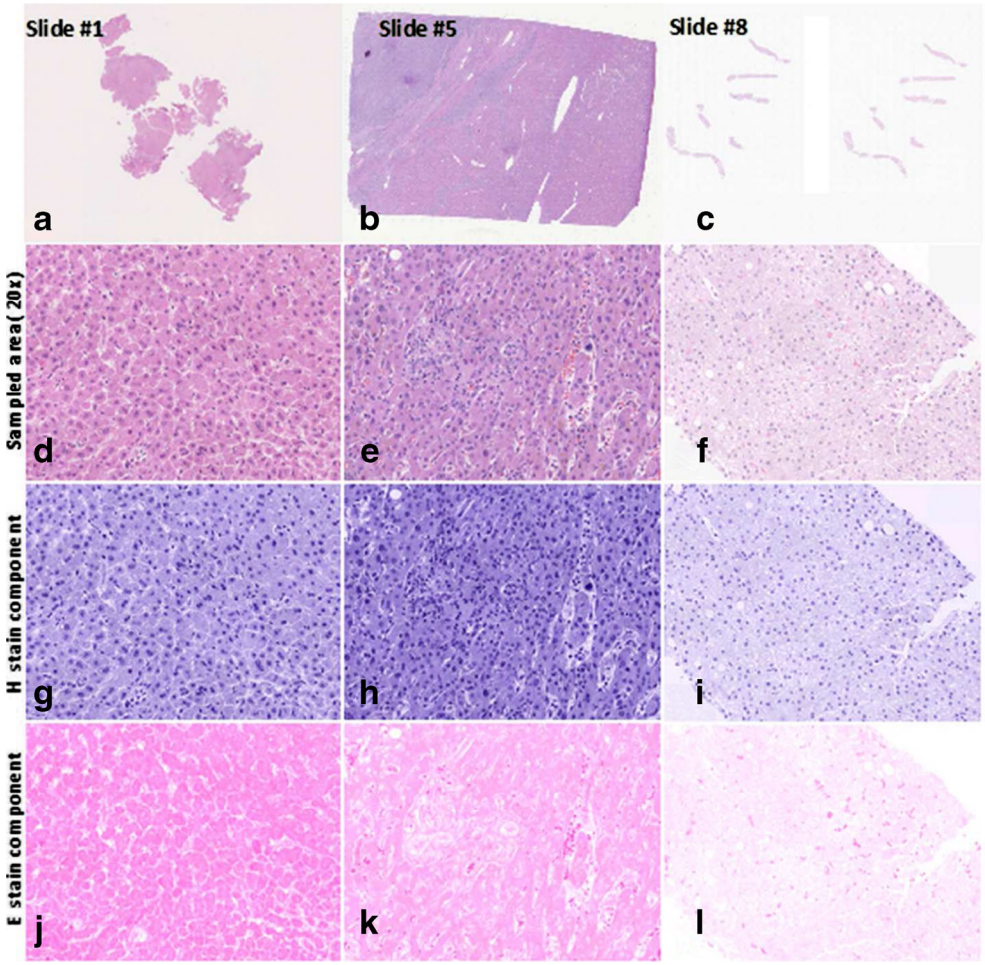

Fig. 2 Illustration of the dye amount variations in different batches of H&E-stained images. **a**–**c** Low-resolution whole slide images; **d**–**f** sampled area from the whole slide images in **a**–**c** at 0.46-μm/pixel resolution (20×). **g**–**i** RGB color representation of the E stain component; **j**–**l** RGB color representation o the H stain component

setting n=21 did not have detrimental effect on the results of the staining correction.

In our experiments, the dye amount table for each slide was estimated using the first ten images sampled from its whole slide image. The cumulative distributions of the H and E dye amounts for the H&E-stained slides #1, #5, and #8 in Fig. 3 show that 95 % of the pixels have dye amounts less than the calculated $c_{\max}$, Eq. 10. Hence, the dye amount LUT drawn based upon the settings of $c_{\min}$ and $c_{\max}$ can be used to effectively transform the input dye amounts to their target values. This also justifies that the default settings for k_c, i.e., k_c=2 works. The resulting negative dye amount values acquired by some of the pixels can be attributed to the limitation of the linear technique employed in the stain decomposition process to capture the staining characteristics of some of the pixels. In determining for $c_{\max}$, Eq. 10, these negative results were mapped to 0.

Staining Correction

We conducted two sets of experiments to investigate the effectiveness of the current staining correction scheme. The first experiment demonstrates how the staining condition of the source slide can be transformed to that of the reference slide, while the second experiment illustrates how the user can recreate his/her preferred staining condition for the slide without necessarily specifying a reference slide. In both cases, we used the Matlab interpolation function, interp1 [26], to map the input dye amounts to their target values.

Staining Correction with a Specified Reference Slide

The LUT for staining correction takes the form $[\mathbf{X}_i^c, \mathbf{Y}_j^c]$, $i \neq j$, where $\mathbf{X}_i^c$ and $\mathbf{Y}_j^c$ are dye amount tables of the cth stain component, c= {eosin (E), hematoxylin (H), and unstained RBC (R)}, for the ith source slide and jth reference slide, respectively. The results of the staining correction are demonstrated in Fig. 4 wherein the uncorrected images are displayed in Fig. 4a and their corresponding stained corrected versions are displayed in Fig. 4b. Each row of images in Fig. 4b correspond to the results of the staining correction for a particular reference slide whose staining condition is represented by the images marked with "ref" in the figure. These results clearly suggest the effectiveness of the present staining correction scheme in minimizing the staining variations in different

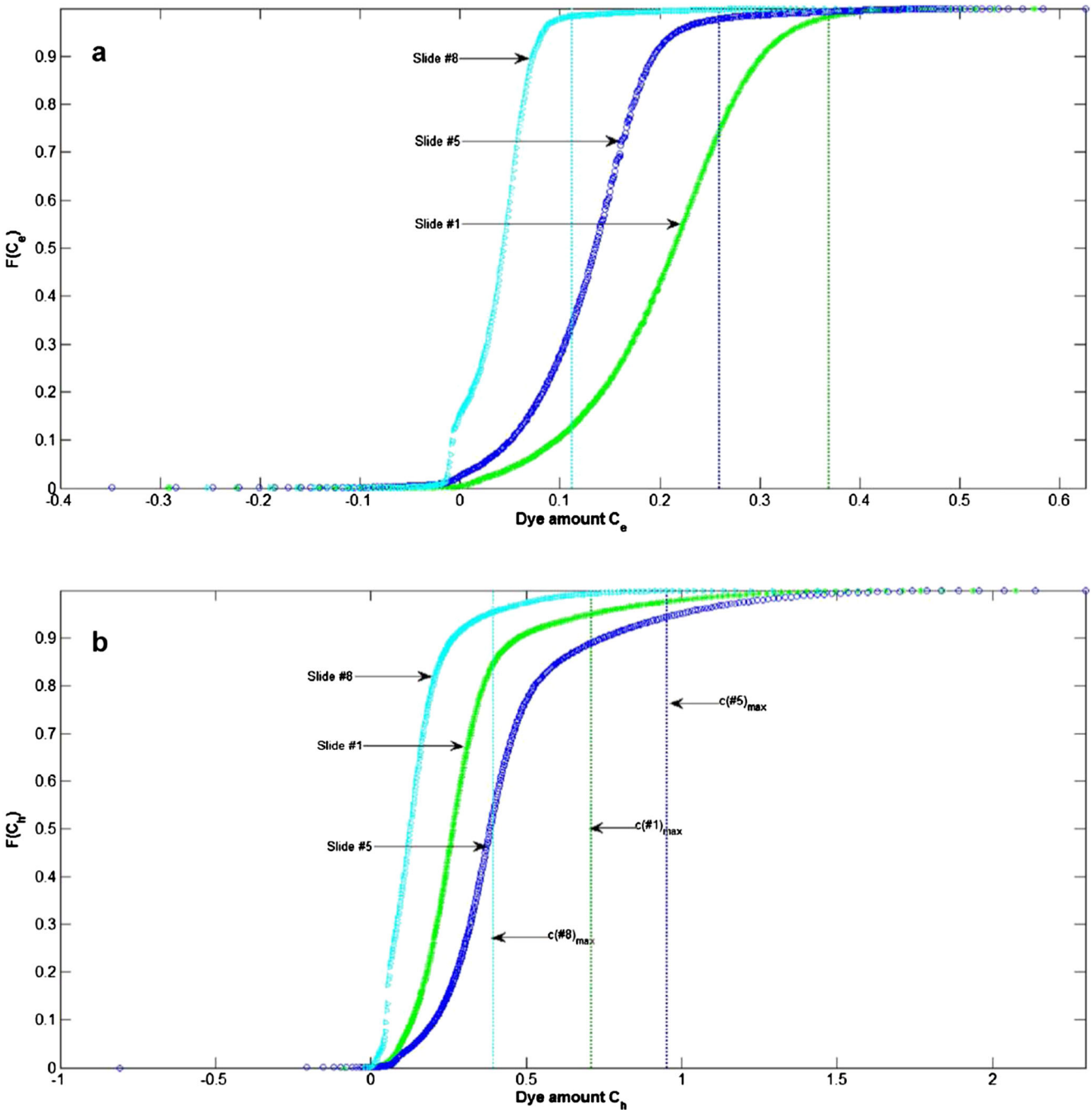

Fig. 3 Cumulative distributions of the dye amounts in three different batches of slides to illustrate the maximum dye amount, c_{max}, settings used to estimate the dye amount tables. **a** E dye amount; **b** H dye amount

batches of histology images regardless of the staining conditions of their slides.

Staining Correction by User Specifications

It was illustrated in the previous section how the staining condition of the source slides can be modified with respect to the staining condition of a reference slide. Such setup is ideal for integration into an image analysis pipeline where we fine-tune the parameters of the statistical classifier using training images. On the contrary, for cases where the purpose of the staining correction is to simply recreate the staining condition preferred by the user, the LUT will take the form $[\mathbf{X}_i^c, \mathbf{X}_j^{c'}]$, $i=j$, where $\mathbf{X}_i^c$ and $\mathbf{X}_j^{c'}$ are the source and target dye amount tables. Here, the target dye amount table is a modified version of the source dye amount table. Let k_h, k_e, and k_r, respectively, refer to the weighting factors introduced to the dye-amount standard deviation of H, E, and R stain components in Eq. 10. While the

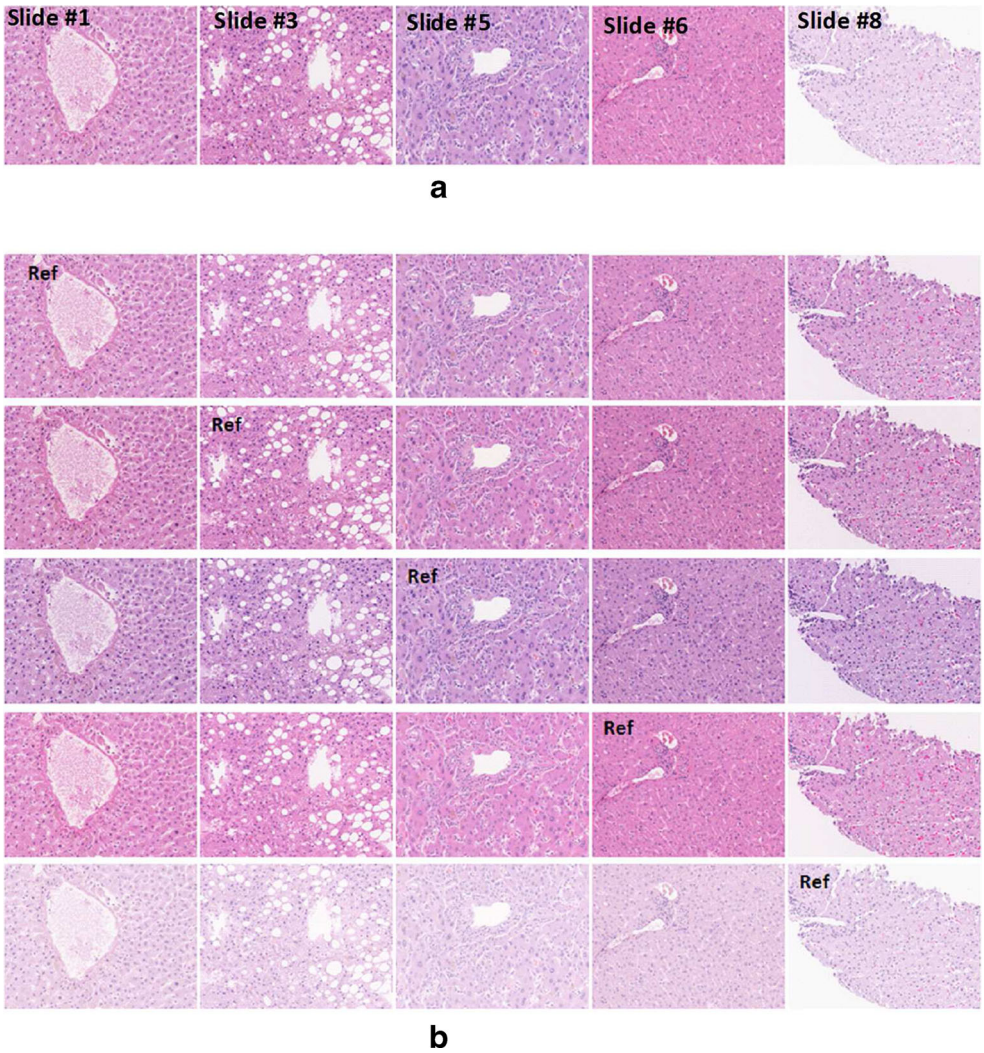

Fig. 4 Results of staining correction on different batches of images. **a** Original H&E-stained images; **b** stain-corrected images

source table $\mathbf{X}_i^c$ is estimated from the result of Eq. 10 with the weighting factors set to their default values, i.e., k_h, $=k_e=k_r=2$, the target dye amount table, $\mathbf{X}_j^{c'}$, is estimated with the user specifying the values for these weighting factors. The user may repeatedly adjust the weighting factors until his/her preferred staining condition is achieved. The results presented in Fig. 5 were generated with the weighting factor for the R stain component was (red blood cell) fixed at $k_r=2$, and only the weighting factors for the H and E were varied. The results demonstrate how we can intuitively recreate different staining conditions by adjusting these weighting factors. For instance, by setting $k_h>k_e$, we will obtain an image which has strong association to hematoxylin staining, or by setting $k_e>k_h$, we will produce an image which expresses close affinity to eosin staining, i.e., the image tends to be more pinkish.

Evaluation

We evaluated the present staining correction scheme in two aspects: (1) color difference of the tissue components from the different slides and (2) tissue classification. We categorized The H&E-stained image pixels into four groups: (i) nuclei, (ii) cytoplasm, (iii) red blood cells (RBC), and (iv) white areas. We collected the training data for these objects by applying *k*-means clustering on the RGB color pixels within the 150×150-pixel image regions which we manually identified from the sample images in the training sets. As these regions may not necessarily contain all the four objects mentioned above, we manually adjusted the number of clusters until we judged that the objects of interest within the region were appropriately clustered. From this process, we collected 7000 RGB color samples for each class. We used these samples to quantitatively evaluate the color difference between the H&E-stained slides before and after staining correction and as training data to classify the image pixels.

Color Difference

The Commission Internationale de I'Eclairge (CIE) [27] defines the color opponent space LAB where *L* defines

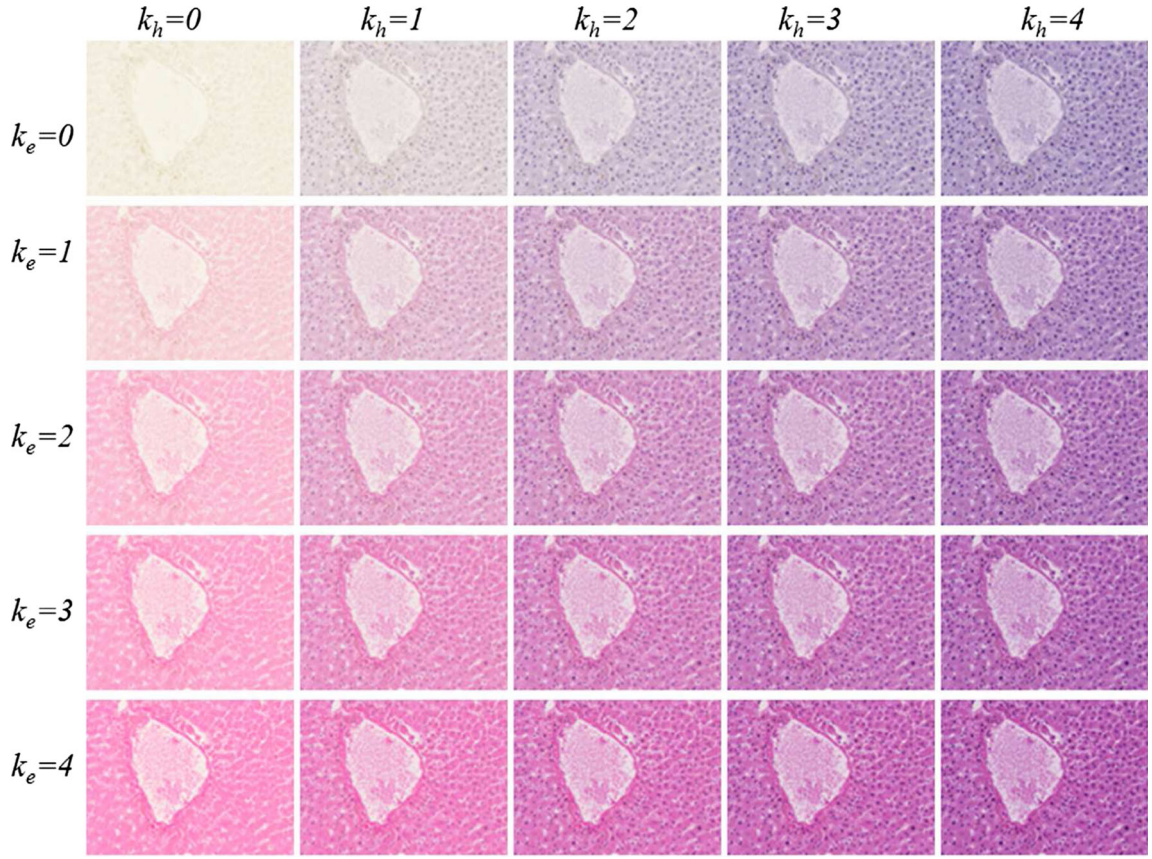

Fig. 5 Illustration on how the user can recreate different staining conditions by varying the dye amount weighting factors, k_h or k_e, in estimating the LUT

the lightness of the pixels, while *a* describes the pixel's redness and *b* the blueness of the pixel. The CIELAB color difference measures the perceptual color difference between two objects. When the CIELAB color difference between two objects is less than three factors, their colorimetric attributes are indistinguishable with the human eyes. The average color difference, $\overline{dE}_{ab}$, between the *i*th source and *j*th reference slide in the CIELAB color space is given by the following expression [15]:

$$\overline{dE}_{ab} = \sqrt{\left(\overline{L}_i - \overline{L}_j\right)^2 + \left(\overline{a}_i - \overline{a}_j\right)^2 + \left(\overline{b}_i - \overline{b}_j\right)^2} \tag{11}$$

where $\left(\overline{L}_i, \overline{a}_i, \overline{b}_i\right)$, and $\left(\overline{L}_j, \overline{a}_j, \overline{b}_j\right)$ are the average *Lab* color values of the RGB color samples from the *i*th and *j*th slides. It

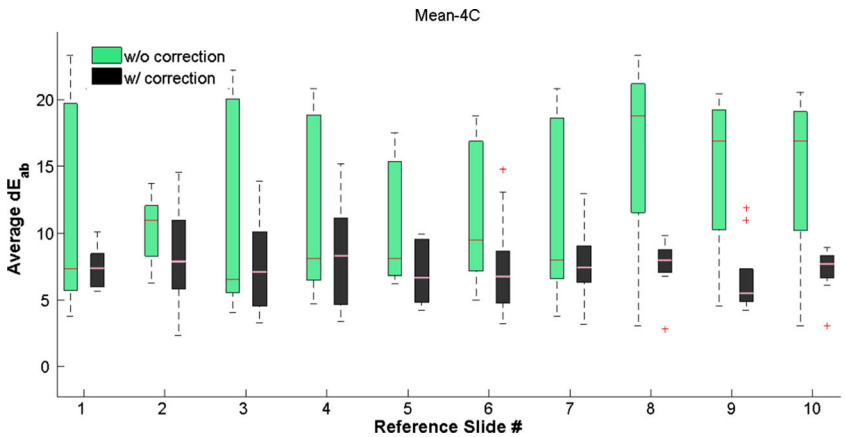

FIg. 6 Color difference before and after staining correction. Variations in the colorimetric attributes of the stained images are depicted by the length of the bars. Application of staining corrections obviously reduces the color difference between different slides

should be noted that since the samples are represented in their RGB color vector, color space transformation from RGB to *Lab* was performed prior to computing Eq. 11 [28].

Figure 6 shows the results of the average color difference measurements between the samples from the *i*th reference slides and the samples from $j=1,2,3..10, j\neq i$ source slides. The box plots show that application of staining correction can reduce the colorimetric variations between the reference and the uncorrected source images. The average reduction in the color difference between the source and reference slides was found to be 9.8 after staining correction was applied. The paired *t* test statistical analysis showed that this reduction is significant at $p<0.001$.

Tissue Classification

Previous works have shown that the accuracy of image analysis is sensitive to variations in the colorimetric attributes of the image [17, 18, 21, 29, 30]. The box plots in Fig. 7 show the average classification results of a linear discriminant classifier as implemented by Matlab [26] on the RGB color samples of nuclei, cytoplasm, RBC, and the white area. The *x* axis corresponds to the *i*th slide training dataset and the *y* axis to the classification results for samples from $j\neq i$, $j=1,2,3..10$ slides. The plots clearly indicate that application of staining correction does not only boost classification accuracies but also provides consistent analysis results for different batches of test images. Application of staining correction improved the classification % accuracy by 16.5 %. Result of the paired *t* test statistical analysis showed that this improvement is significant at $p<0.001$.

Table 1 presents the average classification performance of a linear discriminant classifier. An entry at row *i* and column *j*, $c(i,j)$, denotes the classifier's classification rate for class ω_j given that the actual class of the sample is ω_i. That is, percentage (%) of the samples which are correctly classified is denoted by the diagonal entries, i.e., $i=j$, and those which are misclassified are denoted by the off the diagonal entries, i.e., $i\neq j$. Classification results presented in Table 1 reveal high misclassification rates for nuclei, cytoplasm, and *RBC* samples—nuclei were misclassified to cytoplasm, cytoplasm samples were either misclassified to white or RBC, and RBC samples were misclassified to cytoplasm. Table 2, on the other hand, demonstrates that these misclassifications can be greatly reduced if and when staining correction is implemented prior to tissue classification.

Table 1 Confusion matrix for % classification results of the different tissue components without staining correction

	Nuclei	Cytoplasm	White	RBC
Nuclei	70.626	22.812	3.718	5.688
Cytoplasm	3.189	62.279	23.741	21.582
White	0.001	1.290	98.701	0.016
RBC	2.823	23.729	0.049	73.399

To visualize the impact of the staining variations to the classification of image pixels, classification was also performed on H&E-stained images extracted from the different slides. The result of the classification is a classification map. In the map, image pixels are labeled with distinct colors depending on which class they were assigned to by the classifier, e.g., nuclei-blue, cytoplasm-pink, RBC-yellow, and white-white. Some results of the tissue classification are presented in Fig. 8. High-resolution images of the areas sampled from the H&E-stained slides #5, #6, #8, and #9 are displayed at the first column, while their corresponding classification maps are displayed at the second to fourth columns. The classification maps at the second and third columns were produced when the classifier was trained with samples extracted from different

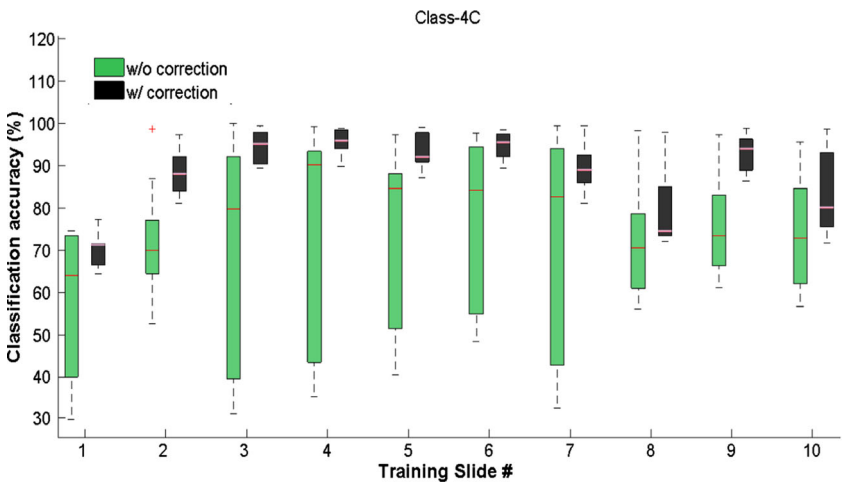

Fig. 7 The impact of the staining variations to classification accuracy. The box plots reveal how the accuracy of a statistical classifier, i.e., linear discriminant classifier, can be impacted by the staining variations in tissue slides. The plot also demonstrate that by integrating staining correction into an image analysis paradigm, we can achieve consistent and accurate classification results across different batches of images

Table 2 Confusion matrix for % classification results of the different tissue components with staining correction

	Nuclei	Cytoplasm	White	RBC
Nuclei	83.32	15.49	0.67	1.04
Cytoplasm	1.09	97.44	1.25	0.46
White	0	0.38	99.62	0
RBC	2.62	19.71	0.59	77.08

slides. The maps at the second column demonstrate the classifier performance when staining correction was not applied, and the maps at the third column demonstrate the effect of the staining correction to the classification accuracies. The maps at the fourth column serve as ground truths for the classification results presented in columns 2 and 3. These were generated when the classifier was trained with samples extracted from the same slide as the test images. The spatial distribution of the color labels in the maps in column 2 significantly vary from their reference maps in column 4. This mainly signifies that most of the pixels were not assigned to their appropriate classes. We can see that these results are in agreement with the classification results presented in Table 1. For instance, when the training data is from slide #5, the cytoplasm areas in slide #8 were misclassified to white areas and those in slide #6 were misclassified to RBC. In contrast, the difference between the maps in columns 3 and 4 is not directly evident, suggesting that the present staining correction scheme could indeed improve the classification accuracy of the tissue components. In general, the results presented herein demonstrate that by integrating staining correction into the histopathology image analysis pipeline, it is possible to achieve consistent level of accuracy for images of different staining conditions.

Discussion

We have presented a method to normalize the staining conditions of histology images by using a look-up table for their pixels' dye amounts. The method was based on the premise

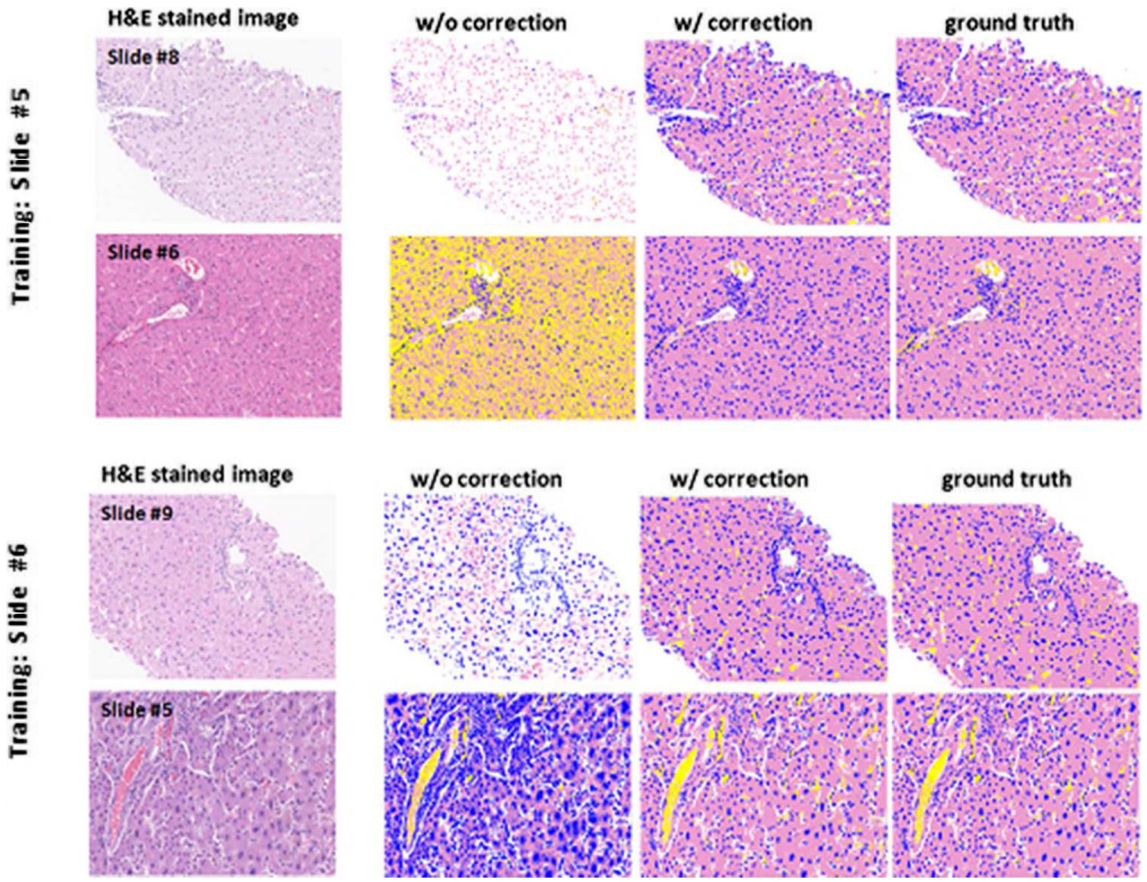

Fig. 8 Classification results for H&E-stained images. The H&E-stained pixels were classified into four classes: nuclei, cytoplasm, RBC, and white. The classifier was trained with the RGB color features of these objects extracted from slides #5 (classifier #5) and #6 (classifier #6). The results of classifier #5 on images from slides #6 and #8 and classifier #6 on images from slides #5 and #9 are presented in columns 2 and 3 of the *upper* and *lower panels*, respectively. The classification maps at the fourth column were produced when classifiers were trained with samples extracted from the same image sets as the input images and served as the ground truth of the classification results presented in columns 2 and 3

that by modifying the dye amounts in stained pixels, we could vary the staining condition of a histology image. Since the present approach does not employ extensive pattern recognition procedures, its computational complexity is comparatively lower than the previously proposed methods. The present method also enables the user to recreate his/her desired staining condition for the given images—a feature which was not available in the previous staining normalization approaches. The effectiveness of the present staining correction approach was demonstrated by the reduction in the overall color difference between the source and reference slide, and by the improvement in the classification accuracies for the different tissue components in the different slides.

Color is an important consideration to the implementation of digital pathology, especially for the automated analysis of stained histology images. Staining correction will have impact on image analysis especially when features such as staining intensity or the staining colors of tissue are used for analysis. In our experiment, the Pearson correlation factor of the CIELAB color differences between the training and test data and the resulting classification accuracies was determined to be −0.85. This result implies that the accuracy of the tissue classification is high when the colorimetric attributes of the training and test data are similar. It would be worth noting that aside from the colorimetric differences between the training and test data, the delineation of the tissue components by their color descriptors is also a major factor that affects the classification results.

There have been several discussions to address the underlying causes of the color variations in digital slides [31–33]. The staining correction we presented in this paper can be used in conjunction with the color calibration slide proposed in [29]. While the use of the color calibration slide ensures that the colors reproduced by the different slide scanners are consistent, the present staining correction scheme addresses the colorimetric differences in histopathology images which are mainly caused by staining variations in histology slides. The present staining method can also be incorporated into the whole slide viewer wherein an option to normalize the staining condition of the slide image can be activated by the user. The selection of the areas from the whole slide image to build the dye amount table can either be done manually or automatically.

Limitations and Future Works

In the present staining correction scheme, dye amount tables were estimated from sample images which were manually sampled from the whole slide images of the tissue slides. For a fully automated implementation of the staining correction, automated extraction of these sample images should be considered. Also, since the determination of the maximum dye amount, c_{max}, is sensitive to the presence of tissue artifacts, such as tissue folds which absorbed more dye than normal tissue areas, integration of methods that automatically detect the presence of tissue artifacts [29] and methods that automatically evaluate the image quality [34, 35] is ideal.

Our experimental results reveal an overall significant reduction in the color differences between the slide images when staining correction was implemented. However, from the classification results presented in Table 2, we can see that the increase in the classification rate for nuclei and RBC is not as high with that of the cytoplasm. We could attribute these results to the estimation of the dye amount tables wherein greater percentage of the image pixels from which the statistics of the dye amounts were computed belong to cytoplasm. Further consideration in the estimation of the dye amount table would be looked into in our future work.

We have utilized H&E-stained samples of liver tissue in our initial experiments. It is expected that the present staining correction scheme is equally effective when applied to other tissue types. The method can also be extended to other types of staining such as special staining or IHC staining.

Conclusions

In histopathology image analysis, the staining pattern of the different tissue components is popularly utilized as features for their classification and segmentation. Variations in the staining conditions of the histology slides can affect the performance accuracy of an image analysis system. We have shown that by correcting the staining conditions of the slides, it is possible to derive consistent and accurate results with simpler classifier design.

The staining correction scheme we introduced in this paper utilizes the dye amount information of the stained pixels. This has the advantage over the previously propose methods which utilizes the stained colors of the pixels in that user can intuitively vary the staining condition of the slide by increasing or decreasing the contribution of the dyes. Furthermore, since the present scheme does not utilized pattern classification methods in the initial step, its computational complexity is lower compared to previously proposed staining normalization methods.

References

1. Yeh FC, Parwani AV, Pantanowitz L, Ho C: Automated grading of renal cell carcinoma using whole slide imaging. J Pathol Inform 4(5): 23, 2014
2. Rizzardi AE, Johnson AT, Vogel RI, et al: Quantitative comparison of immunohistochemical staining measured by digital image analysis versus pathologist visual scoring. Diagn Pathol 7:42, 2012

3. Ghaznavi F, Evans A, Madabhushi A, Feldman M: Digital imaging in pathology: whole-slide imaging and beyond. Annu Rev Pathol 8: 331–359, 2013
4. Walkowski S, Szymas J: Histopathologic patterns of nervous system tumors based on computer vision methods and whole slide imaging (WSI). Anal Cell Pathol 35(2):117–122, 2012
5. Abe T, Hashiguchi A, Yamazaki K, Ebinuma H, Saito H, Kumada H, et al: Quantification of collagen and elastic fibers using whole slide images of liver biopsy specimens". Pathol Int 63:305–310, 2013
6. Ficsor L, Varga VS, Tagscherer A, Tulassay Z, Molnar B: Automated classification of inflammation in colon histological sections based on digital microscopy and advanced image analysis. Cytom A 73(3): 230–237, 2008
7. Karaçali B, Tözeren A: Automated detection of regions of interest for tissue microarray experiments: an image texture analysis. BMC Med Imaging 7:2, 2007
8. Tuominen VJ, Tolonen TT, Isola J: ImmunoMembrane: a publicly available web application for digital image analysis of HER2 immunohistochemistry. Histopathology 60(5):758–767, 2012
9. He L, Long LR, Antani S, Thoma GR: Histology image analysis for carcinoma detection and grading. Comput Methods Prog Biomed 107(3):538–556, 2012
10. Basavanhally AN, Ganesan S, Agner S, et al: Computerized image-based detection and grading of lymphocytic infiltration in HER2+ breast cancerhistopathology. IEEE Trans Biomed Eng 57(3):642–653, 2010
11. Bahlmann C, Patel A, Johnson J, Ni J, et al: Automated Detection of Diagnostically Relevant Regions in H&E Stained Digital Pathology Slides, Proc. SPIE 8315, Medical Imaging: Computer-Aided Diagnosis, February 23, 2012. doi:10.1117/12.912484
12. Pham N-A, Morrison A, Schwock J, Aviel-Ronen S, et al: Quantitative image analysis of immunohistochemical stains using a CMYK color model. Diagn Pathol 2:8, 2007
13. McCann MT, Bhagavatula R, Fickus MC, et al: Automated colitis detection from endoscopic biopsies as a tissue screening tool in diagnostic pathology Image Processing (ICIP), 2012 19th IEEE International Conference on September 30, 2012–October 3, 2012. doi:10.1109/ICIP.2012.6467483
14. Bautista PA, Abe T, Yamaguchi M, et al: Digital staining of pathological images: dye amount correction for improved classification performance. Proc. SPIE Medical Imaging: Computer-Aided Diagnosis, March 30, 2007. doi:10.1117/12.710446
15. Abe T, Murakami Y, Yamaguchi M, et al: Color correction of pathological images based on dye amount quantification. Opt Rev 12:293–300, 2005
16. Kuru K:" Optimization and enhancement of H&E stained microscopical images by applying bilinear interpolation method on lab color mode", Theor Biol Med Model, Feb 6, 2014. doi:10.1186/1742-4682-11-9
17. Murakami Y, Abe T, Hashiguchi A, Yamaguchi M, Saito A, Sakamoto M: Color correction for automatic fibrosis quantification in liver biopsy specimen. J Pathol Inform 4:36, 2013
18. Kothari S, Phan JH, Moffitt RA, Stokes TH, et al: Automatic Batch-Invariant Color Segmentation of Histological Cancer Images. Biomedical Imaging: From Nano to Macro, 2011 IEEE International Symposium on March 30, 2011–April 2, 2011. doi: \10.1109/ISBI.2011.5872492
19. Basavanhally A, Madabhushi A: EM-Based Segmentation-Driven Color Standardization of Digitized Histopathology. *Proc. SPIE* 8676, Medical Imaging 2013: Digital Pathology, 86760G, March 29, 2013. doi:10.1117/12.2007173
20. Niethammer M, Borland D, Marron JS, et al: Appearance normalization of histology slides. Mach Learn Med Imaging Lect Notes Comput Sci Vol 6357:58–66, 2010
21. Khan AM, Rajpoot N, Treanor D, Magee D: Nonlinear mapping approach to stain normalization in digital histopathology images using image-specificcolor deconvolution. IEEE Trans Biomed Eng 61(6):1729–1738, 2014
22. Magee D, Treanor D, Crellin D, et al: Colour Normalization in Digital Histopathology Images. Proc. Opt. Tissue Image Anal. Microsc., Histopathol. Endosc.,100–111, 2009
23. Ruifok AC, Johnston DA: Quantification of histochemical staining by color deconvolution. Anal Quant Cytol Histol 23(4):291–299, 2001
24. Srivastava S, Ha TH, Delp EJ, Allebach JP: Generating Optimal Look-up Tables to achieve complex color space transformations , Image Processing (ICIP), 2009 16th IEEE International Conference on 1641–1644, 2009
25. Bautista PA, Yagi Y: Multispectral enhancement method to increase the visual differences of tissue structures in stained histopathology image. Anal Cell Pathol 35((5-6)):407–420, 2012
26. Matlab Technical Computing Version R2008a
27. Wyszecki G, Stiles WS: Color science concepts and methods quantitative data and formulae, 2nd edition. Wiley, New York, 1982
28. Zhang H, Liu H, Quan S: Hue constrained matrix optimization for preferred color reproduction. J Electron Imaging 21(3):033021, 2012
29. Bautista PA, Hashimoto N, Yagi Y: Color standardization in whole slide imaging using a color calibration slide. J Pathol Inf 5:4, 2014
30. Bautista PA, Yagi Y: Improving the visualization of tissue folds in whole slide images through color enhancement, J Pathol Inform, November 29, 2010. doi:10.4103/2153-3539.73320
31. Badano A, Revie C, Casertano A, ChengWC, et al: Consistency and standardization in medical imaging: a consensus report. J Digit Imaging, 2014. doi:10.1007/s10278-014-9721-0
32. Yagi Y: Color standardization and optimization in whole slide imaging. Diagn Pathol 6(Suppl 1):S15, 2011
33. Shrestha P, Hulsken B: Color accuracy and reproducibility in whole slide imaging scanners. Proc. SPIE Medical Imaging: Digital Pathology, March 20, 2014. doi:10.1117/12.2048769
34. Hashimoto N, Bautista PA, Yamaguchi M, Ohyama N, Yagi Y: Referenceless image quality evaluation for whole slide imaging. J Pathol Inform 3:9, 2012
35. Johnson JP, Krupinski EA, Yan M, et al: Using a visual discrimination model for the detection of compression artifacts in virtual pathology images. IEEE Trans Med Imaging 30(2):306–314, 2011